Polymer Chemistry

ROYAL SOCIETY OF CHEMISTRY

PAPER

View Article Online
View Journal | View Issue

Cite this: *Polym. Chem.*, 2026, **17**, 1592

A novel approach to POx–chelate conjugates and a comparison of their antibacterial activity with POx systems containing amino groups

Marcelina Bochenek, [a] Barbara Mendrek, [a] Agnieszka Kowalczuk, [a] Karolina Olszowska,[a] Łukasz Sieroń,[b] Katarzyna Gawron[c] and Natalia Oleszko-Torbus *[a]

This study presents a novel synthetic strategy for the preparation of antibacterial poly(2-oxazoline)-based (POx) conjugates with chelating agents. A well-defined random copolymer of 2-ethyl-2-oxazoline and 2-[*N*-Boc-5-aminopentyl]-2-oxazoline was synthesized *via* microwave-assisted cationic ring-opening polymerization (CROP). Following deprotection, the copolymer was conjugated with diethylenetriaminepentaacetic acid (DTPA). This work demonstrates a simplified and efficient route to antibacterial POx conjugates, in which amino groups are obtained after polymerization and directly coupled to a chelator. No post-polymerization modification of the polymer is required to generate amino groups in the substituents. Comprehensive characterization of both the conjugated POx and its amino-modified precursor was carried out, including structural analysis and physicochemical properties. Preliminary antibacterial activity and cytotoxicity were assessed, including bacterial membrane assays and microscopic imaging. Both systems exhibited activity against *E. coli*, a commonly used representative Gram-negative strain; however, they act *via* different mechanisms: the conjugate likely acts through cation chelation and its amino-modified precursor through cationic polymer-mediated interactions. Importantly, both polymers were cytocompatible with human fibroblasts. Overall, this study establishes a versatile platform for designing polymeric antimicrobial agents, offering tunable ion-chelating functionality for future biomedical applications.

Received 16th December 2025,
Accepted 5th March 2026

DOI: 10.1039/d5py01190f

rsc.li/polymers

Introduction

Nowadays, infectious diseases constitute a global public health concern, mostly due to the ability of microorganisms to spread and reproduce efficiently.[1,2] Their presence has an impact on healthcare systems, resulting in social and economic burdens, which demand the development and testing of novel antimicrobial systems.[3] In recent years, there has been growing interest in polymers with antibacterial properties,[4–7] among which poly(2-oxazoline)s (POx) have attracted significant attention.[8–10] POx are synthesized *via* living cationic ring-opening polymerization (CROP) of 2-oxazolines, enabling precise control over the molar mass, architecture, and narrow dispersity of the polymer. This controlled 'living' polymerization behavior has been demonstrated under various conditions and monomer/initiator systems, yielding well-defined POx with low polydispersity.[11–14] These polymers have shown great potential in the design of advanced bioactive materials due to their excellent biocompatibility, low immunogenicity, and ease of chemical modification, allowing precise tuning of their properties.[15–24] Typically, the antibacterial activity of POx-based systems is associated with the presence of amino groups introduced into their structure, which can interact with bacterial cell membranes and lead to their disruption.[25] The antibacterial activity of amine-functionalized POx arises primarily from their cationic nature, which disrupts bacterial membranes, much like antimicrobial peptides. Protonated amino or ammonium groups bind to negatively charged bacterial membranes, destabilizing them and increasing their permeability.[8,10,26–29] While this mechanism is dominant for cationic POx, other POx-based systems exert antibacterial effects through alternative strategies, such as DNA targeting, interference with bacterial metabolism, or modulation of bacterial signalling pathways, providing additional approaches to combat resistant pathogens.[30–33]

We previously developed a novel POx-based system containing a chelating moiety with demonstrated antibacterial

[a]*Centre of Polymer and Carbon Materials, Polish Academy of Sciences, M. Curie-Skłodowskiej 34, 41-819 Zabrze, Poland. E-mail: noleszko@cmpw-pan.pl*
[b]*Department of Medical Genetics, Medical University of Silesia, Medyków 18, 40-752 Katowice, Poland*
[c]*Department of Medical Microbiology, Medical University of Silesia, Medyków 18, 40-752 Katowice, Poland*

activity.[34–36] These findings indicated that the antibacterial effect may arise from the ability of the conjugated chelator to bind divalent cations (Ca^{2+} and Mg^{2+}), which play a crucial role in stabilizing bacterial cell membranes. This revealed a new, alternative strategy for achieving antibacterial activity in POx systems through ion chelation. Two conjugation strategies were employed to obtain the POx–chelator system: coupling *via* *N*-hydroxysuccinimide (NHS) ester activation and a reaction using a triazine-based coupling agent. These approaches required the presence of amino groups in POx, which were introduced *via* post-polymerization thio-click chemistry. In the present study, we demonstrate a novel POx–chelator conjugate obtained *via* CROP of a Boc-protected monomer, followed by deprotection and subsequent direct coupling of the chelator, thereby eliminating the need for post-polymerization modification. A well-defined random copolymer of 2-ethyl-2-oxazoline (EtOx) and 2-[*N*-Boc-5-aminopentyl]-2-oxazoline ($PentNH_{Boc}Ox$) was synthesized and designated as POx–Boc. Subsequent deprotection yielded the amino-functionalized copolymer, referred to as POx–NH_2. The complete removal of Boc groups was confirmed, and the absolute molar mass was precisely determined. The selection of monomers for the copolymer design was based on both structural and functional considerations. EtOx was chosen to ensure good aqueous solubility of the resulting copolymer, while $PentNH_{Boc}Ox$ was incorporated to introduce protected amino groups positioned at a distance from the polymer backbone,[37] facilitating their later function. A random copolymer microstructure was employed to distribute the functional monomer units throughout the polymer chain, reducing local density and steric hindrance, which enhances the efficiency of the conjugation reaction. Additionally, this choice of monomer ratio limits the overall content of amino groups in order to minimize potential cytotoxicity and maintain water solubility during the coupling step.[34–36,38] Subsequently, the diethylenetriaminepentaacetic acid (DTPA) chelating agent was attached to the copolymer, resulting in a POx–chelator system (POx–DTPA). The selected chelator was chosen due to its superior metal ion binding efficiency.[39,40] Complete conjugation (substitution of all amino groups with DTPA) and ion-binding capability were confirmed. Importantly, the antibacterial activity of the obtained POx–DTPA conjugate against a model *E. coli* strain was evaluated and compared with its amino-functionalized precursor, which had not been previously studied. This study demonstrates a simplified method for the synthesis of antibacterial POx–chelator systems and provides new insights into the design of metal-ion-scavenging polymeric antimicrobials.

Experimental

Reagents

Methyl 4-nitrobenzenesulfonate (99%, Sigma-Aldrich, St Louis, MO, USA), *n*-propylamine (>99%, Sigma-Aldrich, St Louis, MO, USA), trifluoroacetic acid (TFA, 99%, Alfa Aesar, Haverhill, MA, USA), dichloromethane (DCM, 99.5%, Pure Land Chemical, Shanghai, China), methanol (gradient grade for HPLC, ChemSolve, Tewksbury, MA, USA), ethanol (99.8% for HPLC, POCH S.A., Gliwice, Poland), CaH_2 (95%, Sigma-Aldrich, St Louis, MO, USA), diethylenetriaminepentaacetic acid (DTPA, >99%, Carl Roth GmbH, Karlsruhe, Germany), 4-(4,6-dimethoxy-1,3,5-triazin-2-yl)-4-methyl morpholinium chloride (DMTMM, 97%, Acros Organics, Geel, Belgium), NaOH (pure for analysis, Stanlab Sp. z o.o., Lublin, Poland), $MgCl_2{\cdot}6H_2O$ (pure, POCH S.A., Gliwice, Poland), eriochrome black T (Loba Chemie, Mumbai, India), LiBr (99%, Alfa Aesar, Haverhill, MA, USA), $NaNO_3$ (99%, Thermo Scientific, Waltham, MA, USA), ammonium buffer (pH 10, TarChem Sp. z o.o., Tarnowskie Góry, Poland), $CaCl_2$ (95%, Sigma-Aldrich, St Louis, MO, USA) and ammonium purpurate (murexide, extra pure, Loba Chemie, Mumbai, India) were used as received. $PentNH_{Boc}Ox$ (>97%, Polymer Source, Dorval, QC, Canada) was dried under reduced pressure (1×10^{-4} mbar) using a high-vacuum pump set (nEXT Turbomolecular Pumping Station equipped with an nEXT85H turbomolecular pump and an nXDS6i backing pump, Edwards Ltd, Crawley, UK) for 8 h and stored under an argon atmosphere. EtOx (>99%, Sigma-Aldrich, St Louis, MO, USA) was distilled under reduced pressure, dried over CaH_2, and distilled again. The purity of EtOx was analyzed by gas chromatography (Shimadzu Nexis GC 2030, Shimadzu Corporation, Kyoto, Japan) equipped with two chromatographic lines with FID and BID-2030 detectors and TR-5 (30 m × 0.32 mm ID; 0.25 μm, Thermo Scientific, Waltham, MA, USA) and SH-I-17 (30 m × 0.32 mm ID; 0.50 μm, Shimadzu Corporation, Kyoto, Japan) columns. Acetonitrile (ACN, >99%, Merck KGaA, Darmstadt, Germany) was prepared as described previously.[41] *N*,*N*-Dimethylformamide (DMF) (for HPLC, POCH S.A., Gliwice, Poland) was distilled before use.

Biological reagents

Luria–Bertani (LB) broth (Sigma-Aldrich, St Louis, MO, USA), Mueller–Hinton (MH) broth (Sigma-Aldrich), Dulbecco's modified Eagle's medium (DMEM, Sigma-Aldrich, St Louis, MO, USA), 1-*N*-phenylnaphthylamine (NPN, Sigma-Aldrich, St Louis, MO, USA), trypan blue (PAN Biotech, Aidenbach, Germany) and Triton X-100 (Sigma-Aldrich, St Louis, MO, USA) were used as received. The *Escherichia coli* TOP10 strain was used. Primary dermal fibroblasts (PDFs) were purchased from the American Type Culture Collection (ATCC, Cat. No. PCS-201-010™).

Synthesis of POx–Boc

CROP was carried out in a microwave reactor (Anton Paar Monowave 400, Graz, Austria) at 140 °C. The progress of copolymerization was monitored by nuclear magnetic resonance (^{1}H NMR). Methyl 4-nitrobenzenesulfonate, dissolved in acetonitrile, was placed in a microwave vial equipped with a magnetic stirrer. The copolymer was synthesized *via* a one-pot reaction, in which EtOx and $PentNH_{Boc}Ox$ were added simultaneously to the vial under an argon atmosphere and polymerized. After 2 hours, the reaction was quenched with *n*-propylamine. Following confirmation of total conversion by ^{1}H NMR, the copolymer was purified by evaporation of acetonitrile, dis-

solution in methanol, dialysis (1 kDa Spectra/Por® membranes), and drying under reduced pressure. After purification, the copolymer was named POx–Boc and analyzed by ^{1}H NMR to determine the chemical composition.

Deprotection of POx–Boc

The Boc-protected copolymer was dissolved in DCM, followed by the addition of TFA in a 1 : 1 (v/v) ratio, using a 1.5 mol% excess relative to the Boc groups in the polymer. The reaction was carried out for 1 h at room temperature (RT) under stirring, after which TFA and DCM were evaporated under reduced pressure. The polymer in its salt form, containing trifluoroacetate as the counterion (named POx–$NH_3^+TFA^-$), was used for the conjugation reaction with DTPA. To remove the TFA anion, POx–$NH_3^+TFA^-$ was dissolved in methanol and treated with Amberlyst A-21 ion-exchange resin (Thermo Scientific, Waltham, MA, USA). Then, methanol was evaporated, and the copolymer was purified by dialysis against water (1 kDa Spectra/Por® membranes) and lyophilization. The copolymer containing amino groups (POx–NH_2) was used for cytotoxicity and antibacterial activity studies.

Conjugation of POx–$NH_3^+TFA^-$ with the chelating agent

DTPA (*ca.* 80 eq. per amino group in the polymer) was dissolved in H_2O (c ~1 g mL^{-1}) after the addition of NaOH (5 mol L^{-1}) until the solution reached pH 8.5. DMTMM (*ca.* 5 eq. per polymeric amino group) was dissolved in water (c ~0.05 g mL^{-1}) and added to the aqueous DTPA solution under stirring. Then, an aqueous solution of POx–$NH_3^+TFA^-$ (c ~0.05 g mL^{-1}) was added to the mixture. The reaction solution was stirred overnight at RT, then transferred to a 1 kDa Spectra/Por® membrane and dialyzed against water. The polymer was recovered by freeze-drying and named POx–DTPA.

Measurements

Nuclear magnetic resonance (NMR). ^{1}H and ^{13}C NMR spectra were recorded for samples dissolved in $CDCl_3$ or D_2O using a Bruker Ultrashield spectrometer (Bruker, Billerica, MA, USA) operating at 600 MHz.

Size-exclusion chromatography with multi-angle laser light scattering (SEC-MALLS). Molar mass and dispersity ($Đ$) of the copolymer were determined by SEC-MALLS, using systems operating in DMF. The setup included a multi-angle light scattering detector (DAWN HELEOS II, Wyatt Technologies, Santa Barbara, CA, USA; λ = 663.8 nm) and a refractive index detector (Dn-2010 RI, WGE Dr Bures, Düren, Germany; λ = 620 nm). DMF containing 5 mmol L^{-1} LiBr was used as the mobile phase at a flow rate of 1 mL min^{-1}. The system was equipped with GRAM columns (100 Å, 1000 Å, and 3000 Å) and a guard column (Polymer Standards Service, Germany). Measurements were conducted at 45 °C, and all solutions were filtered using PTFE membranes (0.2 μm) prior to injection. Data acquisition and analysis were performed using ASTRA 7 software (Wyatt Technologies, Santa Barbara, CA, USA).

Determination of the refractive index increment (dn/dc). The refractive index increment (dn/dc) of the copolymer with Boc groups, required for calculating absolute molar masses, was calculated from the equation:

$$\frac{dn}{dc} = w_{PEtOx}\left(\frac{dn}{dc}\right)_{PEtOx} + w_{PBocOx}\left(\frac{dn}{dc}\right)_{PBocOx}$$

where w_{PEtOx} is the weight ratio of 2-ethyl-2-oxazoline in the copolymer and w_{PBocOx} is the weight ratio of 2-[*N*-Boc-5-aminopentyl]-2-oxazoline; $\left(\frac{dn}{dc}\right)_{PEtOx}$ is the refractive index increment of the homopolymer of 2-ethyl-2-oxazoline and is equal to 0.083 mL g^{-1}, and $\left(\frac{dn}{dc}\right)_{PBocOx}$ is the refractive index increment of the homopolymer of 2-[*N*-Boc-5-aminopentyl]-2-oxazoline (measured independently) and is equal to 0.068 mL g^{-1}. The refractive index increment (dn/dc) of the copolymer after the deprotection was calculated from the equation

$$\frac{dn}{dc} = w_{PEtOx}\left(\frac{dn}{dc}\right)_{PEtOx} + w_{PNH_2Ox}\left(\frac{dn}{dc}\right)_{PNH_2Ox}$$

where w_{PEtOx} is the weight ratio of 2-ethyl-2-oxazoline in the copolymer and w_{PNH_2Ox} is the weight ratio of 2-[5-aminopentyl]-2-oxazoline; $\left(\frac{dn}{dc}\right)_{PEtOx}$ is the refractive index increment of the homopolymer of 2-ethyl-2-oxazoline and is equal to 0.083 mL g^{-1}, and $\left(\frac{dn}{dc}\right)_{PNH_2Ox}$ is the refractive index increment of the homopolymer of 2-[5-aminopentyl]-2-oxazoline and is equal to 0.049 mL g^{-1}. The refractive index increments of all homopolymers were determined independently using an SEC-3010 dn/dc refractometer (λ = 620 nm, WGE Dr Bures, Düren, Germany). Five concentrations in DMF were prepared, with a minimum of three measurements per concentration. Data were analyzed using BI-DNDCW software.

Complexometric titration of Ca^{2+} and Mg^{2+} ions. The ability of POx–DTPA to chelate Ca^{2+} and Mg^{2+} ions was studied by complexometric titration. The ability of the conjugate to chelate Mg^{2+} ions was analyzed using the eriochrome black T probe.[42] POx–DTPA was dissolved in water (5 mg mL^{-1}, pH ~5), followed by the addition of $MgCl_2{\cdot}6H_2O$ (in an equimolar amount relative to DTPA in the conjugate). The solution was stirred for 24 hours. After this time, 1 mL of ammonium buffer and 0.15 mL of eriochrome black T solution (in methanol, 5 mg mL^{-1}) were added to the solution. A color change of the solution from transparent to purple was observed. The Ca ion-trapping ability was studied by titration in the presence of murexide as an indicator.[42] The conjugate was dissolved in water (5 mg mL^{-1}, pH ~5), and $CaCl_2$ was added (in an equimolar amount relative to DTPA in the conjugate). The solution was stirred for 24 hours. Then, 0.15 mL of NaOH (5 mol L^{-1}) and 0.15 mL of murexide solution in a mixture of water : ethanol 1 : 1 v/v (2.5 mg mL^{-1}) were added to the solution. A change in the color of the solution from transparent to light purple was observed.

Scanning electron microscopy and energy-dispersive X-ray spectroscopy (SEM-EDX). The presence of complexed ions and mapping of the sample surfaces were performed using scanning

electron microscopy (SEM) coupled with energy-dispersive X-ray spectroscopy (EDX) at 5000× magnification. Samples were prepared on washed and degreased silicon wafers (Cemat Silicon S. A., Bydgoszcz, Poland; with a 3 nm SiO_2 layer) as follows: POx–DTPA was dissolved in water, after which $CaCl_2$ or $MgCl_2{\cdot}6H_2O$ was added in equimolar amounts relative to DTPA units in the conjugate. The mixtures were stirred for 24 h and then dialyzed against water (1 kDa Spectra/Por® membrane). Aliquots of 50 µL were deposited onto the silicon wafers, air-dried for 12 h, and subsequently dried under reduced pressure.

SEM analysis of *E. coli* morphology. The morphology of *E. coli* was analyzed by SEM (Quanta 250 FEG; Thermo Fisher Scientific, Waltham, MA, USA) with a Large Field Detector (LFD) under low-vacuum mode with a beam acceleration voltage of 5 kV. 3 µL of the following solutions were deposited onto silicon wafers: (i) *E. coli* in LB medium (10^8 CFU mL^{-1}); (ii) a solution of POx–DTPA (1 mg mL^{-1} in water) with added *E. coli* (10^8 CFU mL^{-1}), incubated for 2 h at RT; and (iii) a solution of POx–NH_2 (1 mg mL^{-1} in water) with added *E. coli* (10^8 CFU mL^{-1}), incubated for 2 h at RT. The samples were then left to dry overnight under a laminar flow hood. Samples were sputter-coated with a 5 nm gold layer (sputtering time: 10 s, sputtering current: 60 mA) prior to analysis. SEM images were acquired at magnifications ranging from 5000× to 40 000×.

Antibacterial activity assays

Outer membrane (OM) permeability was assessed using NPN (20 µM in PBS) with *E. coli* (OD_{600} = 0.5) incubated with POx–NH_2, POx–DTPA-Ca or POx–DTPA (1 mg mL^{-1}) prior to fluorescence measurement (Ex/Em 355/460 nm) using a Victor X5 plate reader (PerkinElmer, Waltham, MA, USA). POx–DTPA-Ca was prepared as follows: POx–DTPA was dissolved in water, followed by the addition of $CaCl_2$ in equimolar amounts relative to DTPA units in the conjugate. The mixture was stirred for 24 h, dialyzed against water (1 kDa Spectra/Por® membrane) and lyophilized. For inner membrane (IM) permeability assays, *E. coli* suspensions were treated with POx–NH_2 or POx–DTPA (1 mg mL^{-1}), followed by staining with trypan blue (0.4%) and analysis by flow cytometry using a BD FACSAria instrument (BD Biosciences, San Jose, CA, USA; PE channel). Triton X-100 (0.01%) served as a positive control. Results from three independent biological replicates confirmed the trends observed in the NPN and flow cytometry assays.

Determination of minimum inhibitory concentration (MIC)

MICs for POx–DTPA, POx–DTPA-Ca and POx–NH_2 were determined using *E. coli*, applying the microdilution method. A fresh MH broth was prepared, and the bacterial inoculum was standardized to an optical density (OD_{600}) of 0.5, corresponding to approximately 1 × 10^8 CFU mL^{-1}, and then diluted to 1 × 10^6 CFU mL^{-1}. Serial two-fold dilutions of the polymers were prepared in the broth and added to sterile 96-well microtiter plates. Each well contained 100 µL of the polymer solution and 100 µL of the bacterial inoculum, resulting in a final volume of 200 µL per well. Growth controls (broth and inoculum) and sterility controls (broth only) were included. Plates were incubated at 37 °C for 24 h. The MIC was determined as the lowest conjugate concentration that completely inhibited visible bacterial growth, measured at OD_{600} or by visual inspection for turbidity. All tests were performed in three independent biological experiments, each with three technical replicates. MIC values are reported as the average of the three experiments.

Cytotoxicity studies

PDFs were seeded in 24-well plates at a density of 5 × 10^4 cells per well and maintained in DMEM supplemented with 10% FBS, 1% L-glutamine, 1000 U mL^{-1} penicillin, 100 µg mL^{-1} streptomycin, and 250 µg mL^{-1} amphotericin B at 37 °C under a 5% CO_2 atmosphere for 24 h. Subsequently, POx–NH_2 or POx–DTPA (0.1 and 1 mg mL^{-1}) were added to the cultures and incubated for 24, 48, and 72 h. Cell viability was evaluated at each time point using a 10% Alamar Blue solution. Untreated cells served as controls. At each time point, the culture medium was replaced with 200 µL of Alamar Blue solution, followed by incubation at 37 °C for 1 h. After incubation, 100 µL of medium was transferred to a 96-well plate, and cell viability was measured with a VICTOR™ Multilabel Plate Reader (PerkinElmer, Waltham, MA, USA) using a 1 s exposure time.

Results and discussion

Synthesis and characterization of the copolymer precursor (POx–Boc) and its deprotection

Microwave-assisted CROP of $PentNH_{Boc}Ox$ and EtOx, initiated with methyl 4-nitrobenzenesulfonate and terminated with *n*-propylamine, was performed according to the scheme (Fig. 1). The obtained copolymer was named POx–Boc. The characterization of POx–Boc is shown in Table 1.

The total conversion of monomers of POx–Boc was calculated using ^{1}H NMR spectra based on the integration ratio of signals corresponding to protons of methylene groups in the main chain, originating from the monomer and polymer at δ = 4.20–4.24 ppm, δ = 3.79–3.85 ppm and δ = 3.25–3.60 ppm, respectively. M_n shown is the absolute molar mass, determined

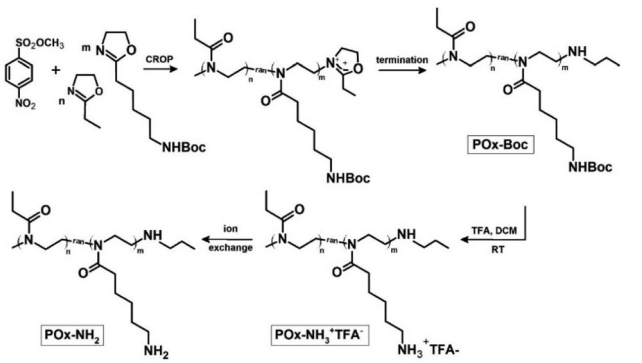

Fig. 1 Scheme for the synthesis of the random copolymer of $PentNH_{Boc}Ox$ and EtOx (POx–Boc), its deprotection (POx–$NH_3^+TFA^-$) and ion exchange (POx–NH_2).

Table 1 Characterization of POx–Boc and POx–NH_2

POx–Boc						POx–NH_2	
$DP_{(t)}$ EtOx : $PentNH_{Boc}Ox$	$M_{n(t)}$ (g mol^{-1})	Conv. (%)	$DP_{(NMR)}$ EtOx : $PentNH_{Boc}Ox$	$M_{n(SEC\text{-}MALLS)}$ (g mol^{-1})	$Đ$	$M_{n(SEC\text{-}MALLS)}$ (g mol^{-1})	$Đ$
70 : 30	14 610	100	70 : 30	15 000	1.45	13 000	1.15

$DP_{(t)}$ – targeted DP; $M_{n(t)}$ – theoretical M_n; Conv. – total conversion of monomers; $M_{n(SEC\text{-}MALLS)}$ – absolute molar masses; $Đ$ – dispersity.

by SEC-MALLS and calculated using the refractive index increment derived from the equations provided in the experimental section. The absolute molar mass of POx–Boc was in good agreement with the theoretical value, and the peak was monomodal (Fig. 2).

The Boc-protecting groups were removed from the copolymer substituents (DCM/TFA, RT), following established procedures,[30,43] yielding POx–$NH_3^+TFA^-$, as depicted in the scheme in Fig. 1. Subsequently, in order to remove the resulting TFA anion, the deprotected copolymer was treated with ion-exchange resins, according to ref. 44, yielding POx with pendant amino functions (POx–NH_2). Quantitative deprotection was confirmed by NMR spectroscopy. Fig. 3 presents the ^1H NMR spectra of POx–Boc and POx–NH_2.

The signal corresponding to the protons of the *tert*-butyl group at δ = 1.45 ppm (signal k) has vanished, thus indicating the total removal of the Boc groups.

A monomodal molar mass distribution was observed for POx–NH_2 (Fig. 2), confirming the successful removal of the protecting groups without polymer degradation. The decrease in the polymer's molar mass, resulting from the detachment of the protecting moieties, was also observed (Table 1).

To briefly summarize, it was possible to quantitatively remove the protective groups from the macromolecular substituents and remove the TFA anion from the copolymer to yield POx with pendant amino groups.

Synthesis of POx–DTPA and the ion-trapping study

The chelating agent DTPA was conjugated to POx–$NH_3^+TFA^-$ using a method based on the triazine-derived coupling agent DMTMM.[45] The reaction scheme is presented in Fig. 4.

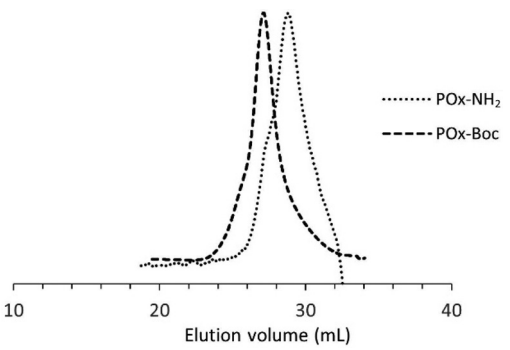

Fig. 2 SEC traces of POx–Boc and POx–NH_2 (DMF with 5 mmol LiBr as the eluent, 1 mL min^{-1}, RI signal).

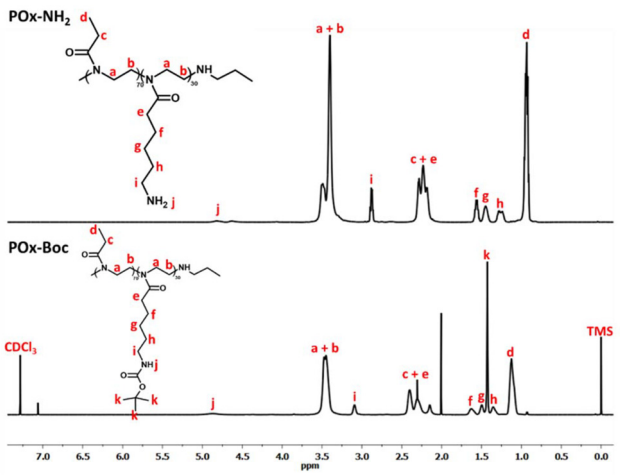

Fig. 3 ^1H NMR of POx–Boc (10 mg mL^{-1} solution in $CDCl_3$) and POx–NH_2 (10 mg mL^{-1} solution in D_2O).

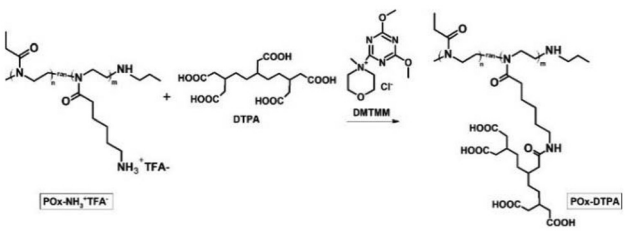

Fig. 4 Scheme of POx–$NH_3^+TFA^-$ and DTPA conjugation leading to POx–DTPA.

After the reaction was completed, the conjugate was designated as POx–DTPA and characterized by ^{13}C NMR (Fig. 5).

The complete substitution with DTPA was confirmed by the shift of the peak originating from the carbon atom of the methylene group at the nitrogen atom from 42.08 ppm to 42.03 ppm. In addition, the shift of the peak in the POx–DTPA spectrum at 177.03 ppm, originating from the carbon atoms of the amide group, and also the shifts of the peaks at 173.26 ppm and 179.57 ppm, derived from the carbon atoms of the carboxyl groups of DTPA, demonstrated the reaction between POx–$NH_3^+TFA^-$ and DTPA. All amino groups in the copolymer (30 mol%) were substituted with the chelating agent DTPA. This design ensures that the density of functional groups is identical in both POx–NH_2 and POx–DTPA, allowing a direct comparison of their activities.

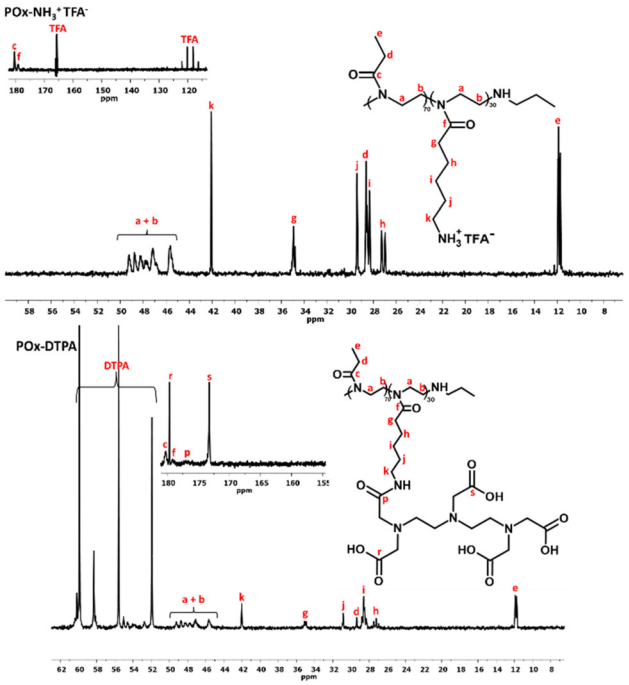

Fig. 5 ^{13}C NMR spectra of POx–$NH_3^+TFA^-$ and POx–DTPA (15 mg mL^{-1} solution in D_2O).

This experiment showed that a chelating agent can be efficiently attached to copolymers obtained *via* the CROP of 2-oxazolines with a protected amino group, followed by deprotection.

The obtained POx–DTPA conjugate was able to entrap model Mg^{2+} and Ca^{2+} ions with 100% efficiency, as confirmed by the eriochrome black T and ammonium purpurate probes, respectively (Table 2). After adding eriochrome black T to the conjugate solution in water, to which an equimolar amount of magnesium ions relative to DTPA in the copolymer had been previously added, the solution immediately changed color from transparent to purple. This color change indicates the absence of free magnesium ions in the solution. Similarly, immediately after the addition of murexide to the solution of POx–DTPA in water, to which an equimolar amount of calcium ions relative to DTPA in the copolymer had been previously added, the mixture turned light purple, indicating the absence of free calcium ions in the solution. The highly efficient trapping of metal ions from solution highlights the strong potential of these polymeric systems.

Table 2 Determination of the chelation capacity of POx–DTPA for Ca^{2+} and Mg^{2+} ions (complexometric titration)

Ions	Mol of DTPA in the sample ($\times10^{-5}$)	Mol of ions added to the sample ($\times10^{-5}$)	Mol of chelated ions ($\times10^{-5}$)	Chelation efficiency (%)
Ca^{2+}	6.23	6.22	6.22	100
Mg^{2+}	6.18	6.08	6.08	100

Following dialysis to remove indicators from the conjugate solutions, the resulting conjugates complexed with calcium and magnesium ions were designated as POx–DTPA-Ca and POx–DTPA-Mg, correspondingly. The pH of the aqueous solution of POx–DTPA with complexed ions increased to 6–7, indicating that carboxyl groups of the chelating agent were involved in the formation of chemical bonds with Ca^{2+} and Mg^{2+}.

Elemental analysis of the samples was carried out using EDX to confirm the presence of ions complexed by the conjugate. The conjugate samples containing complexed calcium or magnesium ions were prepared by drop-casting onto a silicon substrate. Additionally, the spatial distribution of the complexed ions across the substrate surface was analyzed in order to assess their localization within the sample. The EDX spectrum, displaying X-ray energy *versus* intensity, along with the corresponding EDX mapping analysis, is presented in Fig. 6.

A significant increase in signal intensity was observed in the carbon region (0.27–0.28 keV) of the spectra, as well as in the regions corresponding to oxygen (0.53 keV) and nitrogen (0.39–0.40 keV) present in the structure of the tested conjugates. The signal from Si (1.75 keV) was ascribed to the silicon wafer used for sample preparation. Our results confirmed the complexation of Ca and Mg ions with the conjugates, as evidenced by the presence of peaks at energy values characteristic of these ions: 3.69–3.80 keV for calcium and 1.19–1.38 keV for magnesium. These peaks were not observed in the EDX curves of the control POx–DTPA, which was not complexed with metal ions.

The EDX mapping results, shown in Fig. 6B, illustrate the surface coverage of Ca and Mg ions through their characteristic X-ray signals. The uniform distribution of calcium and magnesium ions across the surface of the analyzed sample was observed. Elemental maps were acquired to visualize the spatial localization of these ions, providing insight into how the complexed species are arranged within the conjugate layer. This type of analysis enables qualitative assessment of elemental dispersion and may serve as a basis for further quantitative evaluation.

Comparison of antibacterial activity and *in vitro* cytotoxicity of POx–DTPA and POx–NH_2

To compare the antibacterial activity of POx–DTPA and POx–NH_2, a series of microbiological assays were conducted to evaluate their capacity to disrupt both the IM and OM of a model *E. coli* strain commonly used for preliminary antibacterial screening. These assays included assessments of membrane permeability and integrity, allowing for the investigation of potential differences in the mechanisms of action between the two conjugates. This dual-membrane approach provides a more comprehensive understanding of the antibacterial effects and membrane-targeting capabilities of the tested compounds. Since the number of functional groups is identical in both POx–NH_2 and POx–DTPA, this allows a direct comparison of their activities. Additionally, the activity of POx–DTPA satu-

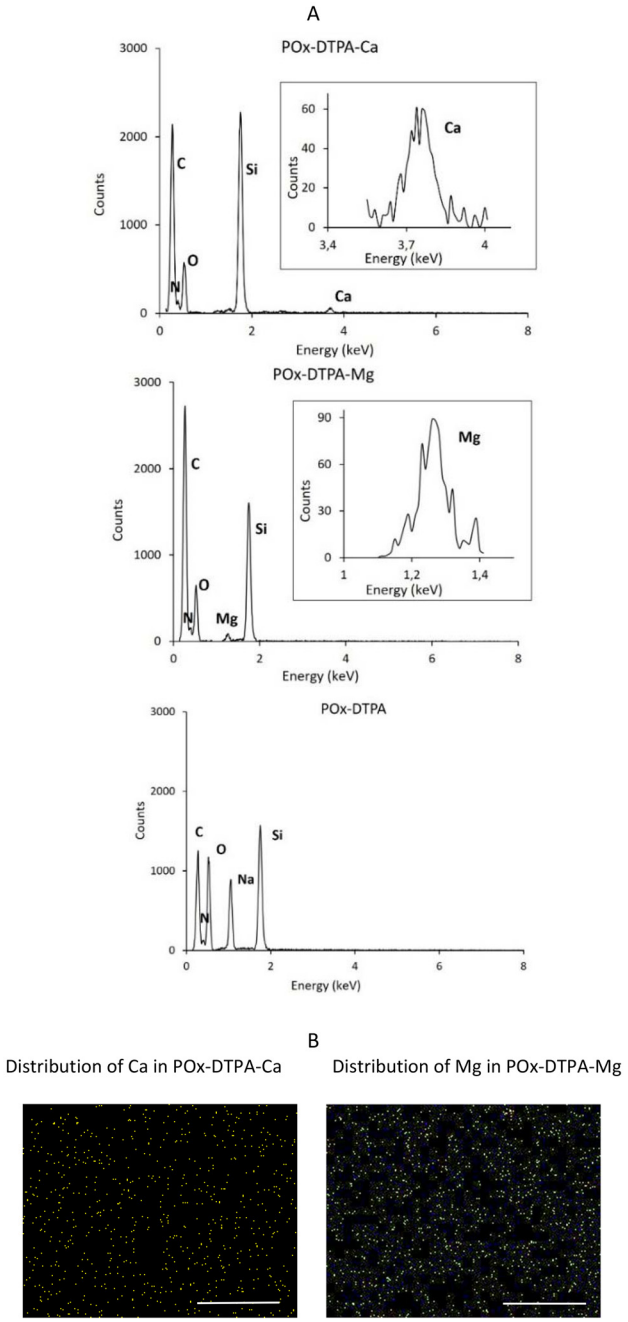

Fig. 6 The EDX curves of POx–DTPA-Ca, POx–DTPA-Mg and POx–DTPA (A); EDX mapping analysis of POx–DTPA-Ca and POx–DTPA-Mg. Elements at the same spot correspond to Ca and Mg, respectively; the scale bar is 20 μm (B). Samples were prepared on silicon wafers from POx–DTPA (10 mg mL^{-1} solution in water) complexed with Ca^{2+} and Mg^{2+} ions in equimolar amounts relative to DTPA units, incubated for 24 h, and air-dried, followed by drying under reduced pressure.

rated with model calcium ions (POx–DTPA-Ca) against *E. coli* was tested.

In the first stage, the minimum inhibitory concentration (MIC) was determined for POx–DTPA, POx–DTPA-Ca and POx–NH_2, using the broth microdilution method against *E. coli*. The MIC is defined as the lowest concentration of an antimicrobial agent that completely inhibits the visible growth of the tested microorganism. POx–DTPA exhibited a MIC value of 0.15 mg mL^{-1}, whereas POx–DTPA-Ca showed a MIC of 1.25 mg mL^{-1}. This indicates a significant reduction in antibacterial activity upon calcium saturation, supporting the role of metal ion chelation in the mechanism of action of POx–DTPA. Literature reports indicate that MIC values of cationic POx-based antibacterial systems against *E. coli* typically range from a few hundredths of mg mL^{-1} to a few mg mL^{-1}, depending on the polymer architecture and mode of action.[46–48] In this context, the MIC value of 0.15 mg mL^{-1} observed for our new chelating system POx–DTPA against *E. coli* places it well within the activity range reported for POx-based antimicrobial systems. The MIC value observed for POx–NH_2 was 1 mg mL^{-1}, indicating that a higher concentration was required to exert a lethal effect compared to POx–DTPA.

To assess the ability of POx–DTPA and POx–NH_2 to damage the integrity of the IM, a trypan blue exclusion assay was conducted. *E. coli* cultures were incubated with the tested polymers (1 mg mL^{-1} of each), followed by staining with the dye. The uptake of trypan blue, indicative of membrane damage, was quantified using flow cytometry. Untreated cells served as a negative control, while Triton X-100, a known membrane-disrupting agent, was used as a positive control for IM disruption.[49] Results are depicted in the fluorescence histograms (Fig. 7).

The fluorescence intensity of *E. coli* cells treated with POx–DTPA and POx–NH_2 and subsequently stained with trypan blue exhibited a noticeable shift toward the fluorescence profile characteristic of Triton X-100-treated bacteria, which is commonly used as a positive control for membrane disruption. This shift indicates a loss of membrane integrity, specifically suggesting an increase in IM permeability. The comparable fluorescence patterns observed for both polymer-treated samples imply that POx–DTPA and POx–NH_2 induce IM permeabilization to a similar extent. These findings are consistent with the ability of both conjugates to facilitate the entry of the otherwise membrane-impermeant trypan blue dye into the cytoplasm, reflecting compromised membrane barrier function.

To evaluate potential damage to the bacterial OM, *E. coli* cultures were incubated with the tested polymers in LB medium (1 mg mL^{-1}) in the presence of NPN dye, followed by fluorescence intensity measurements. NPN is a hydrophobic fluorescent probe that exhibits minimal fluorescence in aqueous environments or in intact bacterial cells. However, upon disruption of the OM, NPN is able to partition into the phospholipid-rich periplasmic space, resulting in a significant increase in fluorescence.[50] This method is widely used to assess the integrity of the bacterial OM and to detect membrane-permeabilizing agents. The fluorescence intensities of NPN observed after treatment with POx–DTPA and POx–NH_2 are presented in Fig. 8. Additionally, this test was also performed for POx–DTPA-Ca (saturated with calcium ions).

An increase in fluorescence intensity was observed in *E. coli* cells treated with either POx–DTPA or POx–NH_2 compared to

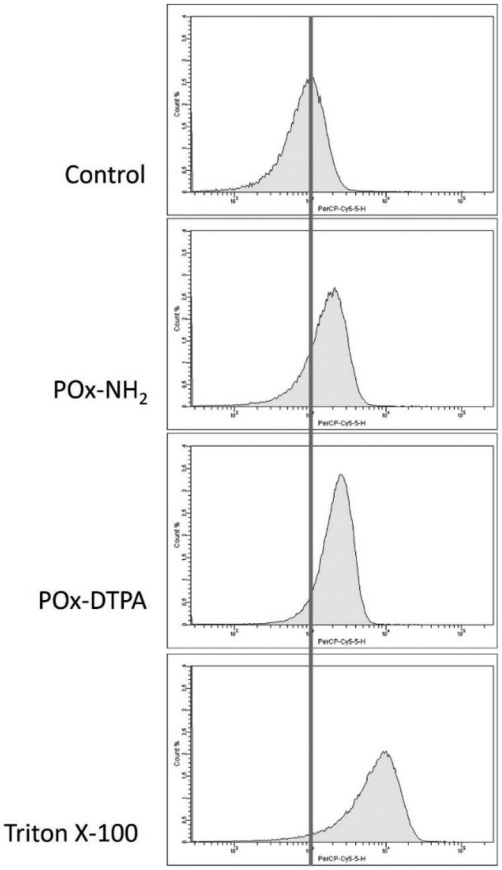

Fig. 7 Flow cytometry analysis of trypan blue staining of *E. coli* treated with POx–DTPA and POx–NH_2. For membrane permeability assays, *E. coli* suspensions were treated with POx–NH_2 and POx–DTPA (1 mg mL^{-1}), followed by staining with trypan blue (0.4%) (Triton X-100 (0.01%) served as a positive control).

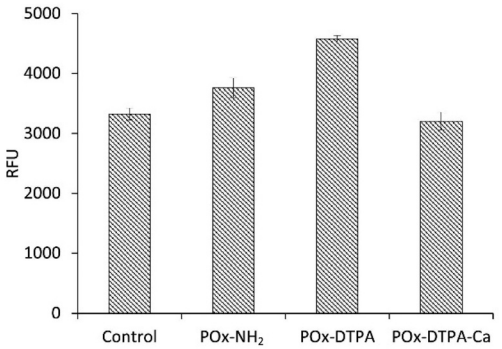

Fig. 8 Relative fluorescence units (RFUs) for *E. coli* cultures treated for 1 h with NPN (20 μM in PBS) in the presence of POx–DTPA, POx–DTPA-Ca and POx–NH_2 (1 mg mL^{-1}) (untreated *E. coli* used as a control).

the untreated control, which indicates disruption of the OM. In contrast, the sample of POx–DTPA pre-saturated with calcium ions exhibited fluorescence intensity at a level comparable to that of the control, indicating that it did not induce outer membrane disruption. Notably, the fluorescence intensity for POx–DTPA was slightly higher than that observed for POx–NH_2.

These findings suggest that both POx–DTPA and POx–NH_2 have the capacity to damage the integrity of bacterial membranes, thereby facilitating the increased uptake of hydrophobic molecules such as hydrophobic dyes. Differences in fluorescence intensity in both copolymer-treated cells may indicate distinct mechanisms of action, possibly related to the

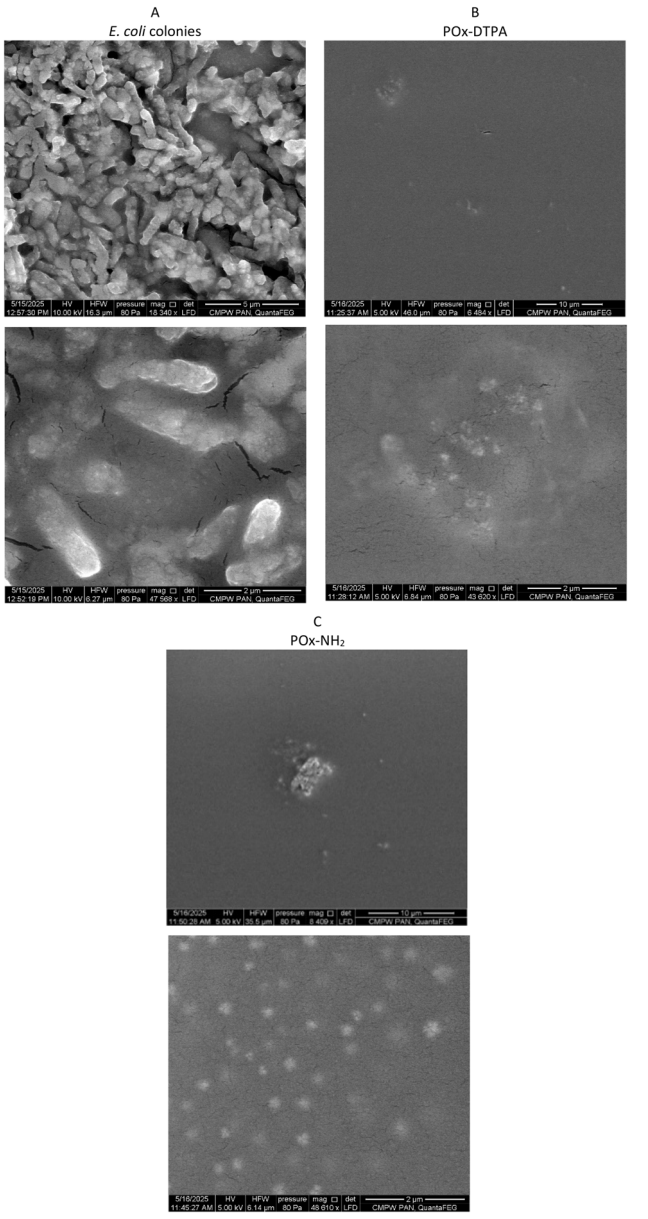

Fig. 9 SEM images of *E. coli* colonies (10^8 CFU mL^{-1}) (A) and polymers incubated with bacteria for 2 h: POx–DTPA (1 mg mL^{-1} in water with *E. coli* (10^8 CFU mL^{-1})) (B) and POx–NH_2 (1 mg mL^{-1} in water with *E. coli* (10^8 CFU mL^{-1})) (C). Samples were prepared by depositing 3 μL of the samples onto silicon wafers, incubating them for 2 h at RT and air-drying. Prior to imaging, the samples were sputter-coated with a 5 nm gold layer.

chelating properties of the DTPA moiety. Specifically, the POx–DTPA conjugate may exert its disruptive effect through the complexation of divalent cations (Ca^{2+} and Mg^{2+}), which are known to play a crucial role in stabilizing the lipopolysaccharide (LPS) layer of the OM of Gram-negative bacteria. This mechanism was indirectly confirmed by the NPN assay, in which calcium-saturated POx–DTPA exhibited no antibacterial activity. In contrast, POx–NH_2, which lacks chelating groups, may interact with the membrane primarily through electrostatic interactions or hydrogen bonding with membrane components, leading to membrane perturbation *via* a different mechanism. Understanding these differences is crucial for tailoring polymer conjugates for targeted antibacterial applications, as the mode of membrane interaction influences both efficacy and specificity. Further studies, including membrane biophysical analyses, would allow the elucidation of the precise molecular interactions that contribute to the enhanced permeabilization induced by POx–DTPA.

To further investigate the antibacterial activity of the tested polymers, SEM analysis was performed. The *E. coli* cultures were incubated for 2 h in the presence of POx–DTPA or POx–NH_2 (1 mg mL^{-1} of each). Next, samples were collected, applied onto solid substrates, air-dried, and subsequently imaged using SEM. As shown in Fig. 9A, dense bacterial colonies are visible prior to exposure to the polymer solutions. After incubation with POx–DTPA or POx–NH_2, no intact bacterial cells were detected (Fig. 9B and C). Instead, only residual debris or fragments of disrupted bacterial cells can be observed, which together indicate effective bactericidal activity and severe membrane damage induced by both tested polymers.

In addition to the studies of the antibacterial activity of the polymer systems, their cytotoxicity toward model human skin fibroblasts was assessed (Fig. 10). The results demonstrated that both POx–DTPA and POx–NH_2 exhibit negligible cytotoxicity within the concentration range corresponding to their antibacterial activity, even after 72 h of exposure. This observation indicates biocompatibility and suggests that the polymer conjugates are safe for potential biomedical applications.

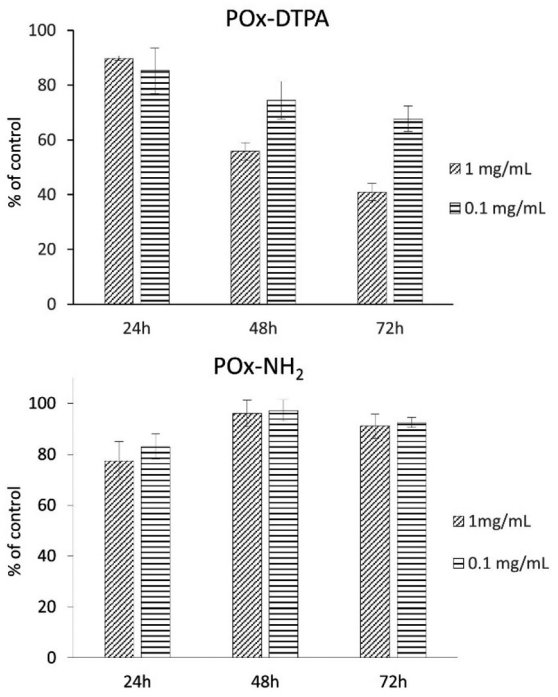

Fig. 10 The cytotoxicity assays of POx–DTPA and POx–NH_2 at 1 and 0.1 mg mL^{-1}, employing model human skin fibroblasts. The results are presented as a percentage of untreated (control) cells, which constituted 100%.

Conclusions

This study demonstrates an efficient route to POx–chelator conjugates *via* direct CROP of functionalized monomers, followed by deprotection and DTPA conjugation, providing a simplified bioactive polymeric platform. Structural characterization confirmed polymer integrity and successful conjugation, while the resulting POx–DTPA effectively chelated divalent cations essential for bacterial membrane stability. Microbiological assays using a model *E. coli* strain revealed efficient inner membrane disruption by both the conjugate and its amino-functionalized precursor, with POx–DTPA causing slightly greater OM damage. In future studies, a broader panel of bacterial strains, including both Gram-negative and Gram-positive species, merits assessment. Both polymers exhibited minimal cytotoxicity, highlighting their potential as versatile antimicrobial materials. The obtained POx system combines structural versatility with tunable monomer composition and functionalization, enabling precise control over physicochemical and biological properties. In this context, the platform presented here serves as a robust foundation for future optimization rather than representing definitive endpoint structures. Taken together, these findings establish POx-based conjugates as a versatile and tunable platform for antimicrobial materials.

Author contributions

All authors contributed to this study. M. B., B. M., and A. K.: synthesis and characterization of the conjugate, analysis of the obtained results, and preparation of the manuscript; K. O.: EDX and SEM analyses; Ł. S. and K. G.: bacteriological studies and cytotoxicity tests; N. O. T.: concept, synthesis and characterization of the conjugate, analysis of the obtained results, and preparation of the manuscript.

Conflicts of interest

There are no conflicts to declare.

Data availability

Repository for open data: https://doi.org/10.18150/PNTKPM.

Acknowledgements

This work was supported by the National Science Centre, project 2021/43/B/ST4/01493.

References

1 D. E. Bloom, S. Black and R. Rappuoli, *Proc. Natl. Acad. Sci. U. S. A.*, 2017, **114**, 4055–4059.
2 Q. Liu, J. Deng, W. Yan, C. Qin, M. Du, Y. Wang, S. Zhang, M. Liu and J. Liu, *Glob. Health Res. Policy*, 2024, **9**, 23.
3 B. Punz, C. Christ, A. Waldl, S. Li, Y. Liu, L. Johnson, V. Auer, O. Cardozo, P. M. A. Farias, A. C. D. S. Andrade, A. Stingl, G. Wang, Y. Li and M. Himly, *Environ. Sci. Nano*, 2025, **12**, 1710–1739.
4 D. Olmos and J. González-benito, *Polymers*, 2021, **13**, 613.
5 S. Alkarri, H. Bin Saad and M. Soliman, *Polymers*, 2024, **16**, 771.
6 S. C. Williams, M. B. Chosy, C. K. Jons, C. Dong, A. N. Prossnitz, X. Liu, H. L. Lopez Hernandez, L. Cegelski and E. A. Appel, *ACS Cent. Sci.*, 2025, **11**, 486–496.
7 R. Bryaskova, N. Philipova, V. Bakov and N. Georgiev, *Appl. Sci.*, 2025, **15**, 1780.
8 M. Zhou, W. Jiang, J. Xie, W. Zhang, Z. Ji, J. Zou, Z. Cong, X. Xiao, J. Gu and R. Liu, *ChemMedChem*, 2021, **16**, 309–315.
9 W. Jiang, M. Zhou, S. Chen, J. Xie, M. Chen, H. Zhang, Y. Wu, X. Chen and R. Liu, *J. Am. Chem. Soc.*, 2023, **145**, 25753–25765.
10 M. Concilio, R. Garcia Maset, L. P. Lemonche, V. Kontrimas, J. I. Song, S. K. Rajendrakumar, F. Harrison, C. R. Becer and S. Perrier, *Adv. Healthcare Mater.*, 2023, **12**, 2301961.
11 S. Borova and R. Luxenhofer, *Beilstein J. Org. Chem.*, 2023, **19**, 217–230.
12 Y. C. M. Wu and T. M. Swager, *J. Am. Chem. Soc.*, 2019, **141**, 12498–12501.
13 C. Petit, B. Grassl, E. Mignard, K. P. Luef, F. Wiesbrock and S. Reynaud, *Polym. Chem.*, 2017, **8**, 5910–5917.
14 C. Guerrero-Sanchez, R. Hoogenboom and U. S. Schubert, *Chem. Commun.*, 2006, 3797–3799.
15 R. Luxenhofer, Y. Han, A. Schulz, J. Tong, Z. He, A. V. Kabanov and R. Jordan, *Macromol. Rapid Commun.*, 2012, **33**, 1613–1631.
16 B. Guillerm, S. Monge, V. Lapinte and J. J. Robin, *Macromol. Rapid Commun.*, 2012, **33**, 1600–1612.
17 W. Wałach, N. Oleszko-Torbus, A. Utrata-Wesolek, M. Bochenek, E. Kijeńska-Gawrońska, Z. Górecka, W. Święszkowski and A. Dworak, *Polymers*, 2020, **12**, 295.
18 S. Jana and M. Uchman, *Prog. Polym. Sci.*, 2020, **106**, 101252.
19 N. Oleszko-Torbus, *Polym. Rev.*, 2022, **62**, 529–548.
20 T. Lorson, M. M. Lübtow, E. Wegener, M. S. Haider, S. Borova, D. Nahm, R. Jordan, M. Sokolski-Papkov, A. V. Kabanov and R. Luxenhofer, *Biomaterials*, 2018, **178**, 204–280.
21 N. Oleszko-Torbus, B. Mendrek, A. Kowalczuk, A. Utrata-Wesołek, A. Dworak and W. Wałach, *Materials*, 2020, **13**, 3403.
22 N. Oleszko-Torbus, M. Bochenek, A. Utrata-Wesołek, A. Kowalczuk, A. Marcinkowski, A. Dworak, A. Fus-Kujawa, A. L. Sieroń and W. Wałach, *Materials*, 2020, **13**, 2702.
23 M. N. Leiske, *Eur. Polym. J.*, 2023, **185**, 111832.
24 A. Lusina, T. Nazim and M. Cegłowski, *Polymers*, 2022, **14**, 4176.
25 N. Oleszko-Torbus, M. Bochenek and A. Kowalczuk, *Polym. Chem.*, 2025, **16**, 2574–2579.
26 W. Jiang, M. Zhou, Z. Cong, J. Xie, W. Zhang, S. Chen, J. Zou, Z. Ji, N. Shao, X. Chen, M. Li and R. Liu, *Angew. Chem., Int. Ed.*, 2022, **61**, e202200778.
27 M. Lin and J. Sun, *Biosaf. Health*, 2022, **4**, 269–279.
28 C. J. Waschinski and J. C. Tiller, *Biomacromolecules*, 2005, **6**, 235–243.
29 M. Zhou, Y. Qian, J. Xie, W. Zhang, W. Jiang, X. Xiao, S. Chen, C. Dai, Z. Cong, Z. Ji, N. Shao, L. Liu, Y. Wu and R. Liu, *Angew. Chem., Int. Ed.*, 2020, **59**, 6412–6419.
30 C. Dai, M. Zhou, W. Jiang, X. Xiao, J. Zou, Y. Qian, Z. Cong, Z. Ji, L. Liu, J. Xie, Z. Qiao and R. Liu, *J. Mater. Sci. Technol.*, 2020, **59**, 220–226.
31 S. Buyuksungur, T. E. Tanir, V. Hasirci and N. Hasirci, *Biomacromolecules*, 2025, **26**, 3139–3154.
32 L. Benski and J. C. Tiller, *Eur. Polym. J.*, 2019, **120**, 109233.
33 A. M. Kelly, V. Kaltenhauser, I. Mühlbacher, K. Rametsteiner, H. Kren, C. Slugovc, F. Stelzer and F. Wiesbrock, *Macromol. Biosci.*, 2013, **13**, 116–125.
34 M. Bochenek, B. Mendrek, W. Wałach, A. Foryś, J. Kubacki, Ł. Jałowiecki, J. Borgulat, G. Płaza, A. Klama-Baryła, A. Sitkowska, A. Kowalczuk and N. Oleszko-Torbus, *Polym. Chem.*, 2024, **15**, 2387–2396.
35 B. Mendrek, A. Kowalczuk, W. Wałach, M. Bochenek and N. Oleszko-Torbus, *J. Mol. Liq.*, 2025, **428**, 127540.
36 M. Bochenek, B. Mendrek, A. Kowalczuk, W. Wałach, Ł. Jałowiecki, J. Borgulat, G. Płaza, J. Kubacki, M. Sikora, A. Fus-Kujawa, Ł. Sieroń, K. Gawron and N. Oleszko-Torbus, *Biomater. Sci.*, 2025, **13**, 3876–3886.
37 S. Cesana, J. Auernheimer, R. Jordan, H. Kessler and O. Nuyken, *Macromol. Chem. Phys.*, 2006, **207**, 183–192.
38 M. Bochenek, B. Mendrek, W. Wałach, A. Kowalczuk, A. Utrata-Wesołek, A. Fus-Kujawa and N. Oleszko-Torbus, *eXPRESS Polym. Lett.*, 2025, **19**, 1226–1237.
39 G. Chauhan, K. K. Pant and K. D. P. Nigam, *Environ. Sci.: Processes Impacts*, 2015, **17**, 12–40.
40 E. Zeini Jahromi and J. Gailer, *Metallomics*, 2012, **4**, 995–1003.
41 N. Oleszko-Torbus, B. Mendrek, W. Wałach, A. Fus-Kujawa, V. Mitova, N. Koseva and A. Kowalczuk, *Polym. Chem.*, 2024, **156**, 742–753.

42 O. Gjems, *Analyst*, 1960, **85**, 738–744.
43 Z. He, L. Miao, R. Jordan, D. S-Manickam, R. Luxenhofer and A. V. Kabanov, *Macromol. Biosci.*, 2015, **15**, 1004–1020.
44 M. Hartlieb, D. Pretzel, K. Kempe, C. Fritzsche, R. M. Paulus, M. Gottschaldt and U. S. Schubert, *Soft Matter*, 2013, **9**, 4693–4704.
45 D. Majonis, I. Herrera, O. Ornatsky, M. Schulze, X. Lou, M. Soleimani, M. Nitz and M. A. Winnik, *Anal. Chem.*, 2010, **82**, 8961–8969.
46 D. Kozon, J. Mierzejewska, T. Kobiela, A. Grochowska, K. Dudnyk, A. Głogowska, A. Sobiepanek, A. Kuźmińska, T. Ciach, E. Augustynowicz-Kopeć and D. Jańczewski, *Macromol. Biosci.*, 2019, **19**, 1–10.
47 C. Krumm, M. Hijazi, S. Trump, S. Saal, L. Richter, G. Georg, G. G. F. K. Noschmann, T.-D. Nguyen, K. Preslikoska, T. Moll and J. C. Tiller, *Polymers*, 2017, **118**, 107–115.
48 C. J. Waschinski, V. Herdes, F. Schueler and J. C. Tiller, *Macromol. Biosci.*, 2005, **5**, 149–156.
49 B. Mattei, R. B. Lira, K. R. Perez and K. A. Riske, *Chem. Phys. Lipids*, 2017, **202**, 28–37.
50 I. M. Helander and T. Mattila-Sandholm, *J. Appl. Microbiol.*, 2000, **88**, 213–219.